[11] A. Y. Cao, X. F. Zhang, C. L. Xu, J. Liang, D. H. Wu, B. Q. Wei, *Appl. Surf. Sci.* **2001**, *181*, 234.
[12] A. Y. Cao, R. Baskaran, M. J. Frederick, K. Turner, P. M. Ajayan, G. Ramanath, *Adv. Mater.* **2003**, *15*, 1105.
[13] S. Huang, A. H. W. Mau, *Appl. Phys. Lett.* **2003**, *82*, 796.
[14] A. Y. Cao, B. Q. Wei, Y. Jung, R. Vajtai, P. M. Ajayan, G. Ramanath, *Appl. Phys. Lett.* **2002**, *81*, 1297.
[15] S. H. Sun, G. W. Meng, Y. W. Wang, T. Gao, M. G. Zhang, Y. T. Tian, X. S. Peng, L. D. Zhang, *Appl. Phys. A* **2003**, *76*, 287.
[16] A. Y. Cao, P. M. Ajayan, G. Ramanath, *Appl. Phys. Lett.* **2003**, *83*, 356.
[17] X. Wang, Y. Liu, G. Yu, C. Xu, J. Zhang, D. Zhu, *J. Phys. Chem. B* **2001**, *105*, 9422.
[18] W. A. de Heer, W. S. Bacsa, A. Châtelain, T. Gerfin, R. Humphrey-Baker, L. Forró, D. Ugarte, *Science* **1995**, *268*, 845.
[19] B. Vigolo, A. Pénicaud, C. Coulon, D. Sauder, R. Pailler, C. Journet, P. Bernier, P. Poulin, *Science* **2000**, *290*, 133.
[20] X. S. Peng, X. F. Wang, J. Zhang, Y. W. Wang, S. H. Sun, G. W. Meng, L. D. Zhang, *Appl. Phys. A* **2002**, *74*, 831.
[21] Y. Huang, X. Duan, Q. Wei, C. M. Lieber, *Science* **2001**, *291*, 630.

Demonstration of Flexible Freestanding All-Polymer Integrated Optical Ring Resonator Devices**

By *Yanyi Huang*,* *George T. Paloczi*, *Joyce K. S. Poon*, and *Amnon Yariv*

Electronic integrated circuits (EICs) face fundamental material and fabrication limitations that are hindering their future use in high-speed telecommunications, optical networking, and optical computing. Alternatively, optical integrated circuits (OICs) are currently receiving more attention for potential use for these and other applications. The materials for advanced OICs will not be limited to semiconductors. Foremost among the new materials, polymers are becoming increasingly important for OIC applications because their optical, mechanical, and functional properties can be broadly tuned by changing their chemical structures through molecular design and proper synthesis procedures. During the past two decades, significant progress was made in polymer materials for OIC applications.[1–3] For example, recently electro-optic polymer materials with highly active nonlinear optical chromophores have been proven to be excellent for use in optical modulator devices.[4–6] However, compared with common materials used today for OIC devices (most of which are semiconductor and inorganic single crystals), polymer materials are not only highly efficient and cheap, but also mechanically flexible. This flexibility is one of the distinct advantages over other materials, making it possible to make pliable and transparent all-polymer devices, and to reshape the devices by adhering to non-flat surfaces for special purposes. Recently, Larsen and co-workers[7] have used soft lithography to make freestanding polymeric structures, which were proposed for use as waveguides, while Steier and co-workers[8] described a method to lift off a thick (> 100 μm) and long (> 2 cm) section of flexible modulator from a solid substrate.

The microring resonator structure is one of the most useful OIC elements. When doped with luminescent dyes, polymer microring resonators can be optically pumped to exhibit lasing.[9–12] The key feature is the dramatic modification of spontaneous emission due to the resonant characteristics of the microring. In addition to lasing, when evanescently coupled to a waveguide, a passive microring resonator acts as an optical filter. The frequency response is typified by a periodic sequence of narrow notches, acting as a highly selective frequency rejection filter. Although several polymeric microring lasers have been produced during the past few years, the studies of polymer microring resonator optical filters have been limited.[13,14]

We report here a simple method to fabricate thin, freestanding all-polymer OIC devices and the successful transfer of the devices to various substrates, such as the curved glass surfaces of capillary tubes. We also demonstrate a passive microring resonator optical filter device with a –27 dB notch extinction for certain wavelengths in the telecommunication band (~ 1.55 μm), which is the best value reported in similar polymer devices and which is within the range of the requirements of practical telecommunications applications.[15] The design and analysis of this filter is based on our previous work on critical coupling between ring resonator and waveguide.[16–20] By utilizing the poor adhesion between the lower cladding polymer and gold, we can easily peel off a very thin layer, several square centimeters in extent, containing a large number of all-polymer OIC devices, with a total thickness of less than 10 μm. The end-facets of the OIC devices can, surprisingly, be easily cut by normal scalpel blades yielding good optical quality inputs and outputs. Each device, or the film of several devices, can also adhere to many different types of surfaces by heating, while the optical properties are minimally changed. This last point is possibly the most significant aspect of freestanding all-polymer OIC devices, setting them apart from their crystalline counterparts.

Figure 1 shows the schematic diagram of the complete procedure for making free-standing OIC devices. A very thin layer of Cr (~ 5 nm) is evaporated onto the freshly cleaned silicon wafer to improve the adhesion between Au (300 nm) and silicon. UV15, an optically clear UV curable epoxy with low refractive index (1.504 at 1550 nm), is applied as the lower cladding layer. SU-8 is a negative ultraviolet photoresist material well known in microelectromechanical systems (MEMS) microfabrication because of its excellent optical and mechanical properties. SU-8 also exhibits excellent sensitivity as an electron-beam resist, and when crosslinked upon electron-beam exposure has a relatively high refractive index (1.565 at

[*] Dr. Y. Huang, G. T. Paloczi, J. K. S. Poon, Prof. A. Yariv
Department of Applied Physics
California Institute of Technology
Pasadena, CA 91125-9500 (USA)
E-mail: yanyi@caltech.edu

[**] Y. H. thanks John M. Choi, William M. J. Green, Prof. Shayan Mookherjea, Dr. Jacob Scheuer, Dr. Yong Xu, and Dr. Reginald K. Lee for fruitful discussions. The work was supported by the National Science Foundation and the Defense Advanced Research Projects Agency.

  DOI: 10.1002/adma.200305813

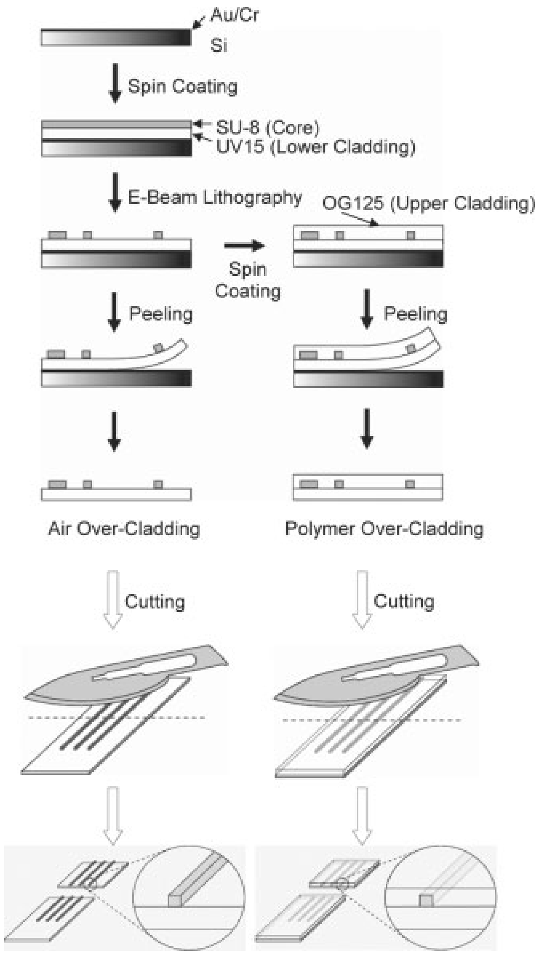

Figure 1. Schematic fabrication procedure for freestanding polymer integrated optical devices. For clarity, the thicknesses are not drawn in proportion to the real devices.

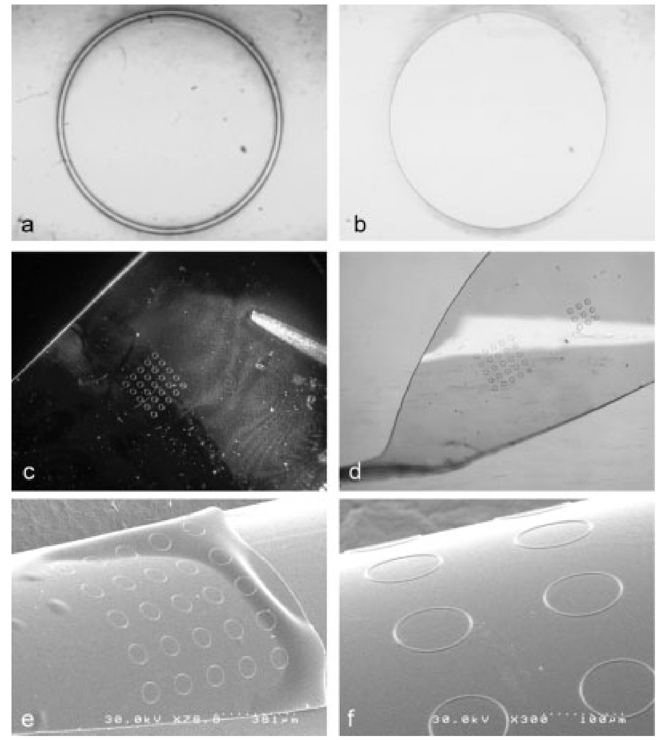

Figure 2. Optical microscopic images of polymeric model structures. All structures are made with SU-8 core layers on UV15 lower cladding using electron-beam lithography. a) Microring with 200 mm diameter and 2 mm wide waveguide. b) Microdisk with 200 mm diameter. c) Freestanding all-polymer film with microring array, illuminated with a HeNe laser. The bright wedge is the fine tip of the tweezers used to hold the film. d) Curved freestanding polymer film with microring array (5 by 5) and microdisk array (3 by 3). e,f) All-polymer microring array on curved surface. The structures are peeled off the substrate and reattached on a glass capillary tube (2 mm diameter) by heating.

1550 nm) and low optical loss for polymeric optical systems.[21] The SU-8 core layer is spin-coated and exposed by electron-beam using a scanning electron microscope (SEM). The structure is dried, without post-baking, by nitrogen gas, after being developed by propylene glycol monomethyl ether acetate. Using the previously mentioned weak adhesion between the UV15 lower cladding layer and the gold, a film of several structures can be easily peeled off from the substrate. To protect the optical devices from contaminants, or to meet refractive-index requirements for the optics, we can also apply an upper cladding polymer, OG125 (refractive index 1.456 at 1550 nm).

We provide in Figure 2 several optical microscope images of our model structures showing the freestanding polymer films prepared using the method described above. In Figures 2a,b, we show a passive microring and microdisk, still on the substrate. Films containing several of these structures are peeled off without damage and become freestanding polymer microring and microdisk arrays, as shown in Figures 2c,d. Once heated to ca. 400 K, perhaps due to localized melting of the polymer surface, the freestanding film can be adhered to surfaces of arbitrary shape or different material. Figures 2e,f show the examples of microring arrays adhered to the curved outer surface of capillary tubes. This way of adhering the polymer films onto arbitrary surfaces is perhaps the easiest way to make non-flat OIC devices. An important use for the adhesion of polymeric optical devices to foreign substrates lies in the potential for hybrid-material devices, i.e., with the polymer devices integrated with semiconductor lasers, or functional materials for chemical or biological sensing.

To be useful in OIC applications, the waveguide sections of the devices must have input and output end-facets of good optical quality, exhibiting low optical loss and good interconnection coupling. Typical of polymer OIC devices, which are left on the silicon substrate, the end-facets are prepared by first dicing the silicon substrate and the polymer with a semiconductor saw, and then polishing the end-facets to produce good optical quality interfaces. An added complication is that the polymer waveguides must be protected, by the use of an encapsulating polymer, from the by-products of the dicing and polishing. Clearly in the case of the films produced by our procedure, there is no substrate to be diced, although dicing or cleaving the substrate before peeling off the optical devices is possible, but only one device can then be put on each substrate. To solve the difficulty of preparing the end-facets of the freestanding polymer waveguides, we find that a simple but effective method is to cut through the film using normal scalpel blades. Both air-clad devices and those with polymer upper cladding layers can be cut easily using scalpel blades. Using optical measurements and SEM observations, we find that the end-facets of the polymer waveguides cut in this fashion are of good optical quality. In principle, one can envision cutting and reassembling polymer optical components to form reconfigurable OICs.

As previously discussed, an important application of microring resonators for wavelength-division multiplexed (WDM) systems is the conditioning and filtering of an input optical waveform. Here we describe a high-performance microring resonator optical filter based on a phenomenon known as critical coupling between a microring and a straight side-coupled waveguide. A schematic diagram of device is presented in Figure 3a. In our previous work, we have shown that this device can be analyzed by a transmission matrix method that describes the evanescent coupling of the optical field into the resonator, and the optical field output as the function of input wavelength.[16–20] When the wavelength is such that the optical phase accumulated in a round trip of the resonator is $2m$, where m is an integer, this is defined as the resonance condition of the microring. In this case, the field returning to the coupler from the ring, after traversing the ring length, interferes destructively with the field impinging on the coupler from the straight waveguide. If the amplitudes of the interfering fields are equal, the destructive interference is complete, and the through output of the straight waveguide vanishes. Mathematically, this complete extinction of the output occurs

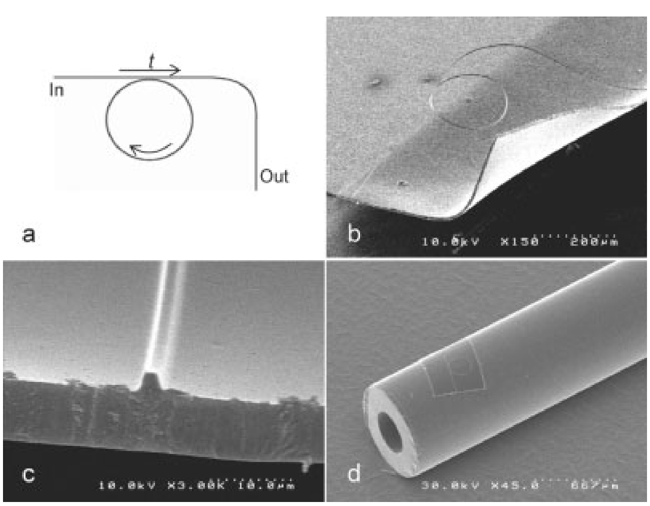

Figure 3. Freestanding all-polymer microring resonator optical filter. a) Schematic diagram of a microring resonator optical filter. b) SEM image of freestanding microring resonator optical filter, purposely curled to show the excellent flexibility. c) SEM image of a waveguide (SU-8) and lower cladding layer (UV15). The end-facet of device is prepared by scalpel-blade-cutting method. d) Polymer microring resonator optical filters on a curved surface. The devices are peeled off of the substrate and heated to adhere to small glass capillary tube (0.8 mm diameter).

at wavelengths right on resonance, when α, defined as the field amplitude remaining after one round trip in the resonator, is equal to $|t|$, the field amplitude that is not coupled into the ring. This equality, $\alpha = |t|$, is referred to as the critical coupling condition,[16–20] and is one of the desired properties of a microring-resonator-based optical filter.

In our experiments, the radius of the microring resonator is designed to be 100 μm, and the width and thickness of the core waveguide 2 μm and 2 μm, respectively. We present, in Figure 3c, an SEM image of the cross-section of a freestanding all-polymer waveguide end-facet as prepared by cutting with a scalpel. The end-facet of the waveguide is smooth. Note that the cross-section does not appear perfectly square due to the electrons backscattered from the lower cladding material during exposure, but this does not adversely affect the optical properties of the waveguide. The total thickness of the device is about 8 μm. As in the case of the microdisk and microring arrays, we can adhere the microring optical filter to the outer surface of a glass capillary tube (0.8 mm diameter). An SEM image of this is presented in Figure 3d, showing minimal change in the physical properties of the device.

The experimental measurement setup and the measured data are presented in Figure 4. One of the key characteristics for a good filter response is, among other things, high extinction of the wavelength rejection nulls in the spectral response, requiring critical coupling, $\alpha = |t|$, of the resonator/waveguide system. Since the loss parameter α is set by the size and waveguiding properties of the ring, we must find the appropriate gap between the waveguide and the resonator to control $|t|$, thus achieving critical coupling. The gap needed to maximize extinction was experimentally found to be 250 nm. Figure 4d shows the measured spectral transfer function of this device in a spectral band that is important for optical communications. Using simple finite difference simulations, we verify that, for wavelengths around 1550 nm, there is only one mode that can propagate through the waveguide structure we have fabricated. By combining the effective refractive index of the single propagating mode, the size of the ring and waveguides, and the waveguide loss, we can fit the data based on matrix methods described previously.[17–20] The theoretical fit is shown as solid line in Figure 4d, and is an excellent fit with experimental data. The numerical fitting parameters are: $\alpha = 0.56$, $t = 0.54$, free spectral range (FSR) is 2.435 nm, and the effective refractive index is 1.508. Based on the output transmission curve, the quality factor (Q) is ca. 2×10^3. In our particular device, the refractive index contrast between core material (SU-8) and lower cladding material (UV15) is low, which increases the bend loss due to decreased confinement. The scattering loss is another main loss source in our device. It is caused by the electron-beam lithography fabrication, and it can be improved by, for instance, reflowing the polymer or other lithography techniques.

The deep notches in the measured spectral response, up to –27 dB (0.2 %) of the maximum signal, to the best of our knowledge, are the lowest values reported for any polymer ring resonator to date, whether on a substrate or freestanding. This

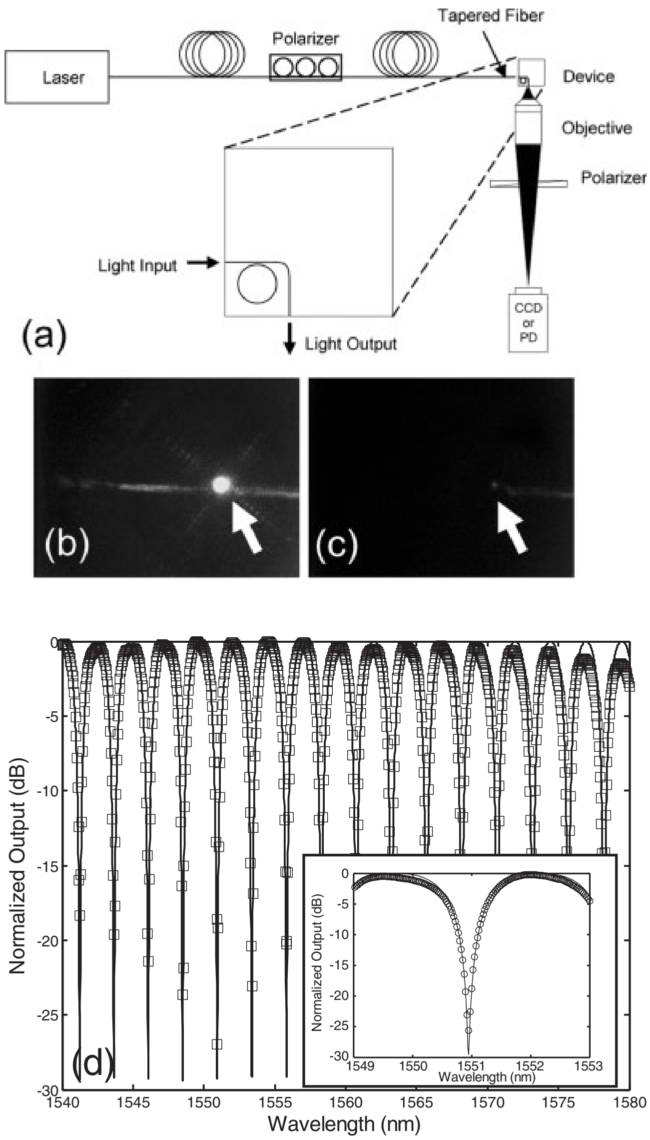

Figure 4. a) Schematic diagram of measurement setup for the microring resonator optical filter. Transverse electric (TE)-polarized laser light is coupled into the input end of polymer device via a tapered fiber, and the output optical signal was collected by an IR-charge-coupled device (CCD) camera or IR photodetector (PD). The two IR-CCD images (b,c) of the output light are at different wavelengths, with the arrows indicating the position of the output end of the device. In (b), the wavelength of the light is off-resonance for the microring and in (c), on-resonance. d) Spectral transfer function of a freestanding air-clad critically coupled microring resonator optical filter. The open square is experimental data and the line is theoretical calculation. The inset is a higher resolution measurement (open circle) around 1550 nm and theoretical calculation (line).

indicates that the properties of the freestanding all-polymer optical filter are as good as can be achieved in a polymer device on a substrate. Furthermore, the value of –27 dB of the maximum response also represents the noise floor of our measurement apparatus, i.e., the photodetector voltage measured when the laser diode is turned off relative to the maximum signal.

In summary, we have developed a novel method to fabricate freestanding flexible all-polymer integrated optical devices with total film thicknesses of less than 10 µm. A microring resonator optical filter, which is demonstrated by this method, shows the most promising results among similar reports and meets the practical rejection requirements of telecommunication systems. This method can be applied to not only to devices fabricated by direct electron-beam writing as described here, but also other fabrication methods such as photolithography and imprint techniques. Further experiments are in progress.

Experimental

Silicon substrates are cleaned by sonicating in isopropanol and dried by nitrogen gas. A 5 nm Cr layer and then 300 nm Au layer are evaporated on those substrates. UV curable polymer UV15 (Master Bond, USA) is spin-coated onto Au and cured by UV light. The core layer of SU-8 epoxy (MicroChem, USA) is spun on the UV15 lower cladding layer. The thickness of SU-8 and UV15 layers are measured to be 2 µm and up to 8 µm, respectively. Electron-beam writing is carried out using a Hitachi S-4100 scanning electron microscope under the control of NPGS (Nanometer Pattern Generation System, J. C. Nabidy Lithography Systems, USA). The structure is developed by SU-8 developer (MicroChem, USA) for 60 s. For devices with polymer upper cladding, OG125 (Epo-Tek, USA) is spun on top of the structures and cured by UV light. The polymer films are peeled off slowly from the metal surface to become freestanding samples. The polymer waveguides are cleaved by scalpel blades to have fine input and output properties.

Optical microscope images are taking through an Olympus BX51 microscope. SEM pictures are taken by a Hitachi S-4100 (Hitachi, Japan) field-emission scanning electron microscope. A tunable laser (8164B Lightwave Measurement System, with 81600B Laser module, Agilent, USA) is employed as the source for the transmission measurements. The laser is input by a tapered/lensed fiber and coupled into one end of the polymer waveguide. The coupling between the input fiber and the polymer waveguide is optimized in each measurement. The optical transmission signal, emitted from the other end of the waveguide is collected by an aspherical objective lens (Newport, USA) and then focused onto an IR-charge-coupled device (CCD) camera (C2741, Hamamatsu, Japan) for imaging. The emitted signal intensity is measured by a femtowatt IR photodetector (2153, New Focus, USA) and acquired by a digital multimeter (2000, Keithley, USA). All the equipment is controlled by MATLAB via general purpose instrumentation bus (GPIB) interface. The signal curve is normalized in each measurement.

Received: August 7, 2003
Final version: October 6, 2003

[1] H. Ma, A. K.-J. Jen, L. R. Dalton, *Adv. Mater.* **2002**, *14*, 1339.
[2] L. Eldada, L. W. Shacklette, *IEEE J. Sel. Top. Quantum Electron.* **2000**, *6*, 54.
[3] S. M. Garner, S. S. Lee, V. Chuyanov, A. Chen, A. Yacoubian, W. H. Steier, L. R. Dalton, *IEEE. J. Quantum Electron.* **1999**, *35*, 1146.
[4] S. R. Marder, B. Kippelen, A. K.-J. Jen, N. Peyghambarian, *Nature* **1997**, *388*, 845.
[5] Y. Shi, C. Zhang, H. Zhang, J. H. Bechtel, L. R. Dalton, B. H. Robinson, W. H. Steier, *Science* **2000**, *288*, 119.
[6] M. Lee, H. E. Katz, C. Erben, D. M. Gill, P. Gopalan, J. D. Heber, D. J. McGee, *Science* **2002**, *298*, 1401.
[7] R. Horvath, L. R. Lindvold, N. B. Larsen, *J. Micromech. Microeng.* **2003**, *13*, 419.
[8] H.-C. Song, M.-C. Oh, S.-W. Ahn, W. H. Steier, H. R. Fetterman, C. Zhang, *Appl. Phys. Lett.* **2003**, *82*, 4432.

ADVANCED MATERIALS

[9] M. Kuwata-Gonokami, R. H. Jordan, A. Dodabalapur, H. E. Katz, M. L. Schilling, R. E. Slusher, S. Ozawa, *Opt. Lett.* **1995**, *20*, 2093.
[10] Y. Kawabe, C. Spiegelberg, A. Schulzgen, M. F. Nabor, B. Kippelen, E. A. Mash, P. M. Allemand, M. Kuwata-Gonokami, K. Takeda, N. Peyghambarian, *Appl. Phys. Lett.* **1998**, *72*, 141.
[11] R. C. Polson, G. Levina, Z. V. Vardeny, *Appl. Phys. Lett.* **2000**, *76*, 3858.
[12] S. X. Dou, E. Toussaere, T. Ben-Messaoud, A. Potter, D. Josse, G. Kranzelbinder, J. Zyss, *Appl. Phys. Lett.* **2002**, *80*, 165.
[13] C. Chao, L. J. Guo, *J. Vac. Sci. Technol. B* **2002**, *20*, 2862.
[14] P. Rabiei, W. H. Steier, C. Zhang, L. R. Dalton, *J. Lightwave Tech.* **2002**, *20*, 1968.
[15] J. V. Hryniewicz, P. P. Absil, B. E. Little, R. A. Wilson, P.-T. Ho, *IEEE Photonics Technol. Lett.* **2000**, *12*, 320.
[16] A. Yariv, *Electron. Lett.* **2000**, *36*, 321.
[17] J. M. Choi, R. K. Lee, A. Yariv, *Opt. Lett.* **2002**, *27*, 1598.
[18] J. M. Choi, R. K. Lee, A. Yariv, *Opt. Lett.* **2001**, *26*, 1236.
[19] A. Yariv, *IEEE Photonics Technol. Lett.* **2002**, *14*, 483.
[20] G. T. Paloczi, Y. Huang, A. Yariv, S. Mookherjea, *Opt. Express* **2003**, *11*, 2666.
[21] W. H.Wong, J. Zhou, E. Y. B. Pun. *Appl. Phys. Lett.* **2001**, *78*, 2110.

Giant Coercive Field of Nanometer-Sized Iron Oxide**

By *Jian Jin*, *Shin-ichi Ohkoshi*,* and *Kazuhito Hashimoto**

Twenty-five centuries ago the first magnet, which was composed of iron ferrite, was discovered. Since then, various iron ferrites such as maghemite (γ-Fe_2O_3) and magnetite (Fe_3O_4) have contributed to our life in numerous fields.[1,2] For technological advances in the future, further improvements of their magnetic properties are desirable. For example, the development of iron ferrites with a large coercive field (H_c) is one of the issues of consequence.[3–5] However, enlarging the H_c value is not so easy in iron ferrites because of their low magnetocrystalline anisotropies. Here we show that a nanocrystal of iron oxide in a silica matrix exhibits a giant H_c value of 2.0 T (1.6×10^6 A m^{-1}) at room temperature. This nanocrystal is composed of a particular phase of iron oxide, ε-Fe_2O_3. The observed H_c value is the largest value so far reported for a metal oxide based magnetic material. The achievement of such a giant coercive field is due to the large magnetocrystalline anisotropy of ε-Fe_2O_3 and the formation of a single magnetic domain by suitably sized nanocrystals.

[*] Prof. S. Ohkoshi, Prof. K. Hashimoto, Dr. J. Jin
Research Center for Advanced Science and Technology
The University of Tokyo
4-6-1 Komaba, Meguro-ku, Tokyo, 153-8904 (Japan)
E-mail: ohkoshi@fchem.chem.t.u-tokyo.ac.jp, hashimoto@fchem.chem.t.u-tokyo.ac.jp

[**] This work was supported by the Japan Science and Technology Corporation (JST), PRESTO (JST), and a Grant for the 21st Century COE Program from the Ministry of Education, Culture, Sports, Science, and Technology of Japan. We thank Dr. Y. Song for helpful discussions, and Mr. T. Hozumi and Dr. H. Mori for help with the TEM experiments.

One way to increase H_c is to decrease the size of the particles forming the single magnetic domain down to the nanoscale region.[6,7] Towards this end, we have prepared iron oxide/silica nanocomposites by combining the reverse-micelle and sol–gel techniques. The crystal structures of the materials obtained were characterized by X-ray diffraction (XRD) spectrometry. Figure 1 shows the XRD patterns for the samples sintered at 900 °C (**1**), 1000 °C (**2**), and 1100 °C (**3**). The patterns of **1** and **3** show the formation of γ-Fe_2O_3 and α-Fe_2O_3 phases, respectively. In contrast, the XRD pattern

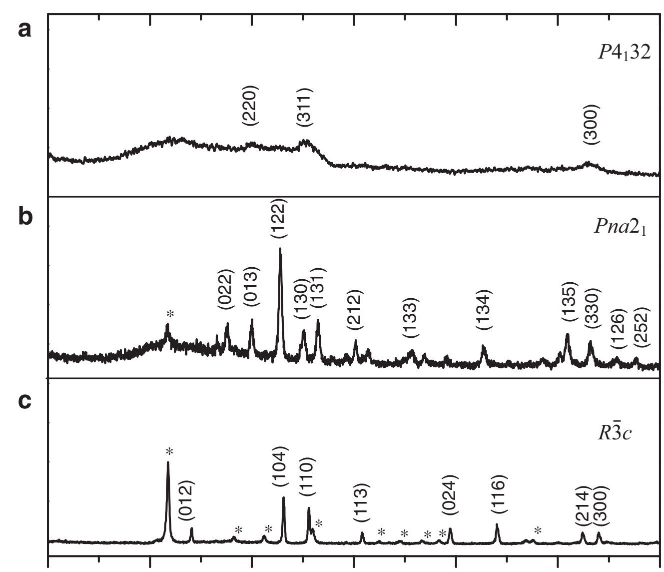

Figure 1. XRD patterns of samples sintered at a) 900 °C (**1**); b) 1000 °C (**2**); and c) 1100 °C (**3**), in which the diffraction peaks indicated by Miller indices corresponding to the space groups of γ-Fe_2O_3, ε-Fe_2O_3, and α-Fe_2O_3 phases are identified. The asterisks represent the peaks of cristobalite (SiO_2).

for sample **2** was completely different from those of the γ- and α-Fe_2O_3 phases. This pattern was determined to be a phase of orthorhombic crystal structure (space group $Pna2_1$; $a = 5.095$ Å, $b = 8.789$ Å, and $c = 9.437$ Å). In the light of XRD references, this crystal was assigned to the ε-Fe_2O_3 phase.[8,9]

Figure 2a shows the transmission electron microscope (TEM; Hitachi H-800) image for sample **2**. It revealed the formation of rod-like nanoparticles with sizes in the range of 100–140 nm in length and 20–40 nm in width. These particles were randomly orientated relative to the Cu grid plane. Selected area energy dispersive X-ray analyses (EDX) confirmed the formation of Fe_2O_3 in the black area surrounded by SiO_2 in the white area. The high-resolution TEM (HRTEM) image recorded on an individual nanoparticle showed good crystallization and clear lattice fringes (Fig. 2b and its insets). The observed lattice plane space between the arrowheads is 6.50 Å, which corresponds to the distance between two (011) planes of ε-Fe_2O_3. The Fourier transform analysis of the HRTEM image proved that the long axis of the particle is the *a*-axis of the ε-Fe_2O_3 crystal.

  DOI: 10.1002/adma.200305297